ANL-ART-268

Modeling support for the development of material surveillance specimens and procedures

Applied Materials Division

ANL-ART-268

Modeling support for the development of material surveillance specimens and procedures

---

prepared by
Mark C. Messner, Argonne National Laboratory

Applied Materials Division

September 2023

Abstract

This report describes modeling and simulation activities performed at Argonne National Laboratory supporting the development of passively actuated mechanical test articles for material surveillance in Molten Salt Reactors (MSRs). These test articles are a critical technology in formulating material surveillance programs for future MSRs to monitor the degradation in the structural properties of the materials in critical plant components. The main activity described in this report is the development of a method for inferring the amount of mechanical damage a test article has experienced during some duration of exposure to plant thermal and environmental conditions, using only mechanical test data collected from the test articles before and after exposure. The basic approach is to develop a model of the test article, including a description of mechanical degradation through continuum damage mechanics, and then use this model to cast the problem of inferring mechanical degradation in the test article materials into a shooting problem for a set of ordinary differential equations. We can then solve the shooting problem to determine the amount of damage accumulated in the sample. The report also details a few miscellaneous simulation studies completed at Argonne to support the development of the test articles themselves at Idaho National Laboratory.

Table of Contents

List of Figures

List of Tables

1 Introduction

This report describes modeling support for the ART program effort to develop passively actuated, thermally loaded surveillance test articles for monitoring the degradation of structural materials in Molten Salt Reactor (MSR) plant environments. The main experimental and sample development effort for this general task is being completed at Idaho National Laboratory (INL). In FY24, Argonne National Laboratory (ANL) provided modeling and simulation support to assist INL in developing the surveillance articles and the associated acceptance criteria and practices that will be required to implement a material surveillance program at a future operating MSR.

Argonne's work focused on developing a procedure for determining the remaining life of a test article, exposed to previous thermal cycling, using information potentially available from ex situ testing on previously-exposed samples. This procedure provides a means for a plant operator to remove a sample from the reactor, do some out-of-reactor testing, and use those results to infer the remaining life of the test article and the corresponding structural component. Chapter 2 describes such an approach. This method formulates a mathematical model for the test article, using a continuum damage mechanics model to represent creep-fatigue degradation in test section. With this formulation, inferring the current state of damage in the test section can be posed as a shooting problem — an optimization problem to solve for the initial conditions of the simulation. Chapter 2 develops this approach and demonstrates its effectiveness using synthetic (simulated) test data.

Argonne also completed a variety of analyses for INL to support the development of the test articles. Chapter 3 summarizes some of these analyses, which include calculations related to ratcheting and out-of-plane deformation in the test articles and on the effect of the large thermal transient required to bring the test articles to room temperature, prior to any ex-situ testing.

Finally, Chapter 4 summarizes Argonne's FY23 work and discusses future work to finalize practices and procedures for actually implementing a material surveillance program based on passively actuated surveillance specimens.

2 Inferring damage from ex situ tests

2.1 Description of the problem

2.1.1 Inferring material degradation

As noted in Chapter 1, the main objective of ANL's work in FY23 is to determine a way to infer the current amount of material damage/degradation in a surveillance sample based on information potentially available from a surveillance campaign. The general approach we focus on here envisions the following process:

1. The operator completes pre-service, potentially destructive testing on some number of surveillance test articles. The goal of this pre-service testing would be to establish a baseline for the undamaged response of both the test articles as a system and the surveilled material in particular. Likely this testing would consist of furnace thermal cycling using Digital Image Correlation (DIC) or some other means to monitor the strain the test section combined with some amount of standard creep and creep-fatigue testing on the surveilled material.

2. The operator inserts a number of surveillance test articles into the reactor, in a location where the test article experience representative environmental conditions and the temperature fluctuations in the reactor translate into representative or bounding mechanical load on the test section of the articles.

3. Periodically, the operator removes one or more test articles from the reactor, for example during outages, and conducts some amount of ex situ mechanical testing to characterize the current, degraded material response. Here we envision this testing to be instrumented thermal furnace cycling. These tests would heat up and cool down a sample in a furnace, recording the strain on the test section as a function of time.

Given this mode of operation, the key question is: can we use the post-service, ex situ testing and the pre-service, ex situ testing to determine the remaining life of the surveillance test article and, by proxy, the remaining life of the monitored component?

2.1.2 Continuum damage mechanics

One way to predict the remaining life of the material is to first predict the amount of prior damage the material accumulated and then use a damage model to predict the remaining life. This chapter describes a means to predict the current amount of damage in the material, as parameterized by a continuum damage model, given the information available from the surveillance program, outlined above.

Continuum damage mechanics is a mathematical description of material degradation and failure. The key concept is a damage parameter or damage fraction, d. If $d = 0$ the material is completely undamaged, if $d = 1$ the material has failed. Mathematically, models for the material behavior apply the damage fraction to degrade the current elastic properties of the material. So if the undamaged Young's modulus of the material is E the damaged Young's modulus is $(1 - d)E$. This damaged modulus expresses the ability of the material to carry

Parameter	Value	Units
l_1	1	in
l_2	4	in
$l_3 = l_1 + l_2$	5	in
r_1 ($A_1 = \pi r_1^2$)	0.125	in
r_2 ($A_2 = \pi r_2^2$)	0.25	in
r_3 ($A_3 = \pi r_3^2$)	0.30	in

Table 2.1: Geometric parameters describing the test article geometry used in this study.

load: if $d = 0$ the material has the original elastic modulus; if $d = 1$ the modulus is zero and the material cannot transmit stress.

Given the current damage parameter d and the expected future service loads on a component we can infer the remaining life of that component using a damage model. For example, the ASME Boiler & Pressure Vessel Code uses a time fraction creep damage model based on Larson-Miller correlations for creep damage, Miner's rule and strain-based fatigue curves for fatigue damage, an a bilinear creep-fatigue interaction diagram for creep-fatigue loading.

For many high temperature components the fatigue damage is comparatively low. For these situations we can consider only creep damage to control the component life. We adopt this perspective here. Future work could extend the approach developed in this chapter to true creep-fatigue interaction.

2.2 Synthetic data

We do not have a complete dataset of the type envisioned in the previous section. Instead, to test various methods of inferring the current material damage, we develop a synthetic dataset, representative of the types of data available in an operating surveillance campaign. To do so we simulate the response of a test article exposed to fluctuating temperatures.

For these examples we assume a test article made of 316H steel and Alloy 617. 316H is the surveilled material and so makes up the test section and the case section of the sample. Alloy 617 is then the driver material. Figure 2.1 shows a conceptual view of the test article, which could represent any generation of the actual test articles under develop: large, cylindrical samples, small cylindrical samples [1, 2], or the flat specimens under development at INL [3].

Table 2.1 describes the geometry parameters used in this study. These are representative of the small, cylindrical design tested at ANL.

2.2.1 Material models

To simulate the response of the test article under repeated thermal cycling we need models for high temperature deformation and creep damage in 316H and Alloy 617.

2.2.1.1 Deformation

We apply a fairly simple model to describe plastic and creep deformation in both alloys. Previous work [4] describes the details of the model, which switches between a rate indepen-

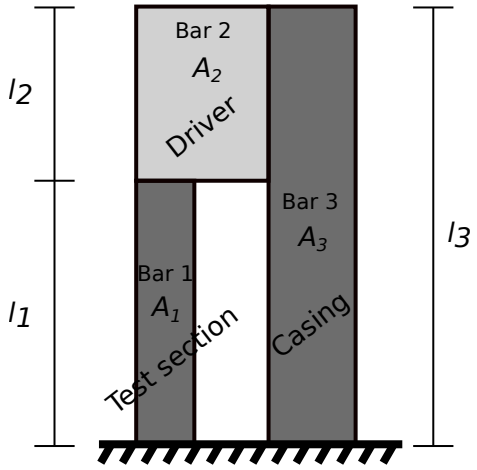

Figure 2.1: Sketch of the three bar model used to represent the surveillance test articles. This model can represent any of the several generations of surveillance articles under development at ANL and INL. The model represents the length of the casing section with an arbitrary parameter l_3, but for all actual specimen designs $l_3 = l_1 + l_2$

dent response and a rate-dependent viscoplastic response as a function of temperature and strain rate. That previous work also describes how the key parameters were determined for 316H and Alloy 617 from experimental data.

The model is based on the theory of Kocks and Mecking [5]. The model decomposes the total strain rate into the sum of elastic, inelastic, and thermal strains

$$\dot{\varepsilon} = \dot{\varepsilon}_e + \dot{\varepsilon}_{in} + \alpha \dot{T} \tag{2.1}$$

with $\dot{\varepsilon}$ the total strain rate, $\dot{\varepsilon}_e$ the elastic strain rate, $\dot{\varepsilon}_{in}$ the inelastic strain rate, α the temperature-dependent instantaneous coefficient of thermal expansion, and $\dot{T}$ the temperature rate. The elastic strain rate follows from Hooke's law:

$$\dot{\varepsilon}_e = \frac{\dot{\sigma}}{E} \tag{2.2}$$

with $\dot{\sigma}$ the rate of the engineering stress and E the temperature-dependent Young's modulus.

Reference [4] describes the flow rule, which switches between a rate independent and rate dependent response based on the normalized Kocks-Mecking activation energy:

$$\dot{\varepsilon}_{in} = \begin{cases} \dot{\varepsilon}_{ri} & g \leq g_0 \\ \dot{\varepsilon}_{rd} & g > g_0 \end{cases} \tag{2.3}$$

where

$$g_0 = \frac{kT}{\mu b^3} \log\left(\frac{\dot{\varepsilon}_0}{\dot{\varepsilon}}\right) \tag{2.4}$$

Parameter	316H	Alloy 617	Units
A	-3.35	-8.679	-
B	-3.23	-0.744	-
C	-5.82	-5.41	-
g_0	0.771	0.538	-
b	2.02	2.48	Å
$\dot{\varepsilon}$	3.3×10^9	3.3×10^{13}	1/hr
k	1.38064×10^1	1.38064×10^1	MPa Å / K

Table 2.2: Flow rule parameters for the two materials.

with k the Boltzmann constant, T absolute temperature, μ the temperature-dependent material shear modulus (calculated as $\mu = E/(1+2\nu)$ using $\nu = 0.31$ and the temperature dependent Young's modulus), b a representative length scale (taken to be a Burgers vector), and $\dot{\varepsilon}_0$ a reference strain rate.

The rate dependent flow rule is the Perzyna model defined by

$$\dot{\varepsilon}_{rd} = \left\langle \frac{\sigma - K}{\eta} \right\rangle^n \text{sign}\left(\sigma\right) \tag{2.5}$$

with

$$n = -\frac{\mu b^3}{kTA} \tag{2.6}$$

and

$$\eta = e^B \mu \dot{\varepsilon}_0^{-1/n} \tag{2.7}$$

with A and B material parameters and where K is isotropic hardening, defined by a Voce model

$$\dot{K} = d\left(R - K\right)\left|\dot{\varepsilon}_{in}\right| \tag{2.8}$$

with d and R temperature dependent material parameters.

The rate independent flow rule is the standard 1D formulation with a yield stress of

$$\sigma_y = \mu e^C \tag{2.9}$$

with C a material parameter and the same Voce isotropic hardening rule. As described in [4] the key to this formulation is ensuring the isotropic hardening parameter K remains consistent between the two flow rules.

We choose to describe the state of the material with the stress σ and the isotropic hardening K. This means refactoring Eqs. 2.1 and 2.2 to give an equation for the stress rate:

$$\dot{\sigma} = E\left(\dot{\varepsilon} - \dot{\varepsilon}_{in} - \alpha\dot{T}\right) \tag{2.10}$$

Table 2.2 lists the flow rule parameters used here for 316H and Alloy 617. Figure 2.2 plots the temperature-dependent elastic and thermal properties (a) and Voce hardening parameters (b) for the two materials.

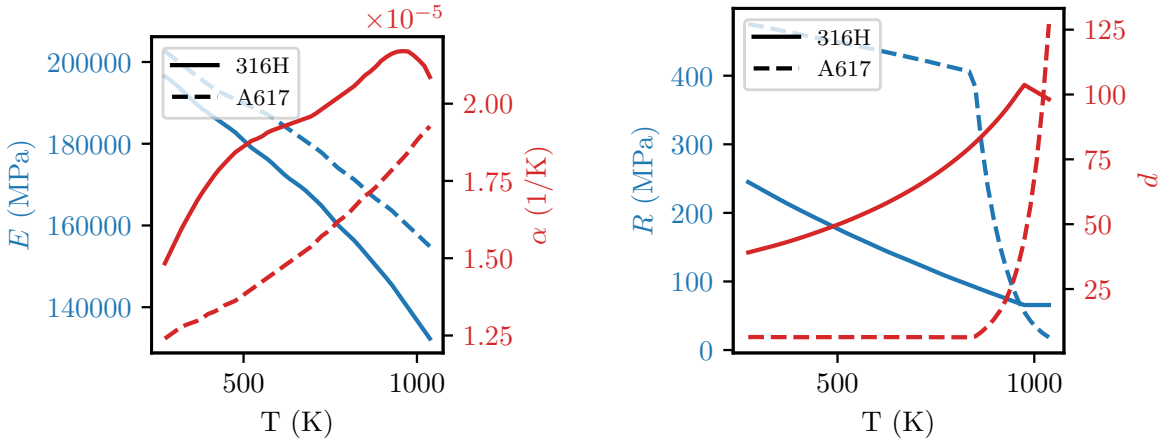

(a) Thermoelastic properties

(b) Isotropic hardening parameters

Figure 2.2: Thermoelastic (a) and isotropic hardening (b) parameters for the deformation models for 316H and Alloy 617.

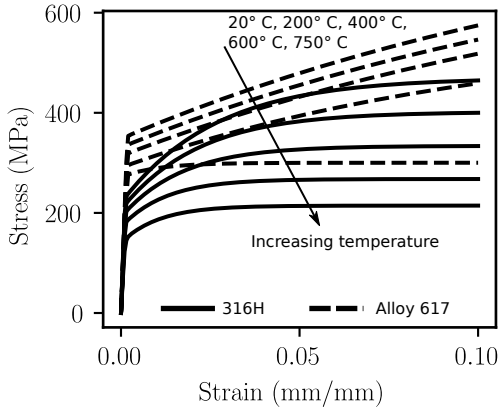

Figure 2.3: Predicted flow curves under uniaxial tension for both models as a function of temperature.

Figure 2.3 then plots predicted tensile curves for the two materials at a strain rate of 8.33×10^{-5} 1/s as a function of temperature. The predicted flow stresses for the two materials are reasonable compared to experimental measurements.

This model only has isotropic hardening, which means it may not accurately predict long-term cyclic behavior in either alloy. However, it is a reasonable starting point for predicting damage in the surveillance articles, particularly for load histories with long holds at constant conditions (for example, plants that operate more like current light water reactors, as opposed to load following designs).

2.2.1.2 Damage

This deformation model can be modified to account for the development of creep damage in the 316H test section of the surveillance article. Changing the previous equations to account for material degradation with a continuum damage model requires only three modifications:

1. Replace the Young's modulus E with the modified Young's modulus $E' = (1 - d)E$.
2. Replace the stress σ with the modified stress $\sigma' = \frac{\sigma}{1-d}$ in the flow rule[1].
3. Supplement the equations with a time evolution rule for damage giving $\dot{d}$ as a function of stress, temperature, and the inelastic flow rate.

In the following we will consider two damage models. The first is a trivial model defined by

$$\dot{d} = 0. \tag{2.11}$$

However, we consider this in the context of the complete system of ODEs describing the material response, where the initial value of damage d_0 might not be zero. That is, this model describes a material that has underwent prior damage, but where damage does not continue to further evolve during the simulations.

The second model is based on the time-fraction, Larson-Miller creep damage model used in Section III, Division 5 of the ASME Code. A linear Larson-Miller model relates stress to the time to rupture and the absolute temperature with the formula:

$$A_{LM} \log_{10} \sigma + B_{LM} = T \left(\log_{10} t_R + C_{LM} \right) \tag{2.12}$$

where t_R is the time to rupture and A_{LM}, B_{LM}, and C_{LM} are material parameters, with C_{LM} being the Larson-Miller coefficient relating temperature and time in the rupture correlation. The time-fraction damage model relates the creep damage fraction to the time to rupture at the current stress:

$$d = \int_0^t \frac{dt}{t_R} \tag{2.13}$$

or

$$\dot{d} = \frac{1}{t_R}. \tag{2.14}$$

[1] We would need to make a similar substitution in the hardening rule if it depended on the stress. However, the Voce rule does not depend on stress except through the already-modified flow rule.

Parameter	Value
A_{LM}	-5379.0
B_{LM}	29316.3
C_{LM}	15.94

Table 2.3: Larson-Miller damage model for 316H. Units are compatible with MPa for stress and hours for time.

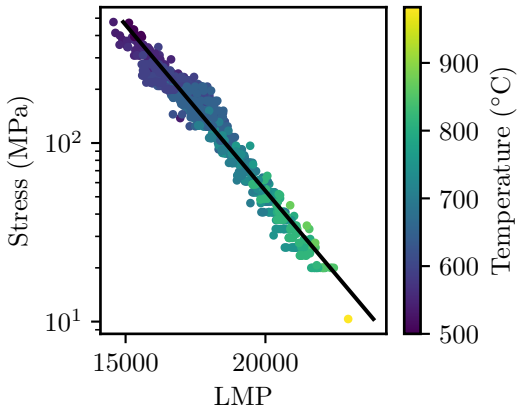

Figure 2.4: Larson-Miller fit to 316H rupture data underlying the Larson-Miller continuum damage model used here.

Combining Eqs. 2.12 and 2.14 provides a continuum damage model with the form:

$$\dot{d} = 10^{C_{LM} - B_{LM}/T} \, |\sigma|^{-A_{LM}/T} \, . \tag{2.15}$$

We assume that the size of the driver and casing sections, relative to the test section, keeps the stress in these two regions of the surveillance article low enough to prevent the development of significant creep damage. This means we only need to simulate damage in the test section, made from 316H. Table 2.3 lists calibrated material coefficients for this continuum damage model for 316H. These coefficients derive from a Larson-Miller fit to a large creep rupture database for 316H, summarized in Figure 2.4. These parameters represent average creep rupture over the database, i.e. not a lower bound as in the ASME Boiler & Pressure Vessel Code.

2.2.2 Structural model of the test article

So far we have described a complete constitutive model, as a system of ODEs, for a single material point under uniaxial load. To describe the three bar system we need to develop a coupled system of ODEs describing the response of all three sections: the test, driver, and casing sections. Ideally we want this system of ODEs to be as small as possible to reduce the amount of time required to simulate the system response and, especially, to infer the current level of damage as described below. In particular, as we are only interested in the behavior of the test section we can factor out the equations describing the stress/strain response of the other two pieces of the test article.

As described by Figure 2.1 in the subsequent derivation we label the test section bar 1, the driver section bar 2, and the casing section bar 3. The lengths of these three sections are l_1, l_2, and l_3 with $l_3 = l_1 + l_2$ in the actual test articles. The cross-section areas of these three sections are similarly A_1, A_2, and A_3, the stress in each section σ_1, σ_2, σ_3, etc. Remember from above we only apply the damage model to bar 1.

The fundamental equations describing the response of the system are:

- The evolution equations for the stress in the three bars: $\dot{\sigma}_1$, $\dot{\sigma}_2$, and $\dot{\sigma}_3$, from Eq. 2.10.
- The evolution equations for the isotropic hardening in the three bars: $\dot{K}_1$, $\dot{K}_2$, and $\dot{K}_3$, from Eq. 2.8.
- The evolution equation for the damage in bar 1: $\dot{d}$, from Eq. 2.11 or 2.15.
- The constraint equation representing equilibrium between bars 1 and 2:

$$\sigma_1 A_1 = \sigma_2 A_2. \tag{2.16}$$

- The constraint equation representing equilibrium between bars 2 and 3:

$$\sigma_2 A_2 = -\sigma_3 A_3. \tag{2.17}$$

- The constraint equation representing overall strain compatibility between bars 1, 2, and 3:

$$\varepsilon_1 l_1 + \varepsilon_2 l_2 = \varepsilon_3 l_3. \tag{2.18}$$

After simplifying out redundant equations the complete response of the three bar system can be described with six coupled ODEs describing:

1. The stress in bar 1:

$$\dot{\sigma}_1 = M \left[\frac{l_3}{l_1} \dot{\varepsilon}_{in,3}(\sigma_3, K_3, T) - \frac{l_2}{l_1} \dot{\varepsilon}_{in,2}(\sigma_2, K_2, T) - \dot{\varepsilon}_{in,1}(\sigma_1', K_1, T) + \alpha' \dot{T} \right] \tag{2.19}$$

2. The temperature of the entire system:

$$\dot{T} = \hat{\dot{T}}(t) \tag{2.20}$$

3. Damage in bar 1, defined by either Eq. 2.11 or 2.15, as a function of σ_1 and T
4. Isotropic hardening in bar 1:

$$\dot{K}_1 = d_1 \left(R_1 - K_1 \right) \left| \dot{\varepsilon}_{in,1} \left(\sigma_1', K_1, T \right) \right| \tag{2.21}$$

5. Isotropic hardening in bar 2:

$$\dot{K}_2 = d_2 \left(R_2 - K_2 \right) \left| \dot{\varepsilon}_{in,2} \left(\sigma_2, K_2, T \right) \right| \tag{2.22}$$

6. Isotropic hardening in bar 3:

$$\dot{K}_3 = d_3 \left(R_3 - K_3\right) \left|\dot{\varepsilon}_{in,3}\left(\sigma_3, K_3, T\right)\right| \tag{2.23}$$

where

$$M = \frac{E_1'}{1 + \frac{E_1' A_1 l_3}{E_3 A_3 l_1} + \frac{E_1' A_1 l_2}{E_2 A_2 l_1}}, \tag{2.24}$$

$$E_1' = (1-d)E_1, \tag{2.25}$$

$$\sigma_1' = \frac{\sigma}{1-d}, \tag{2.26}$$

$$\alpha' = \alpha_3 \frac{l_3}{l_1} - \alpha_2 \frac{l_2}{l_1} - \alpha_1, \tag{2.27}$$

$$\sigma_2 = \frac{A_2}{A_3}\sigma_1, \tag{2.28}$$

and

$$\sigma_3 = -\frac{A_1}{A_3}\sigma_1 \tag{2.29}$$

The driving force in this coupled system is the rate of change in temperature as a function of time, $\hat{\dot{T}}(t)$. Specifying this function and initial conditions for each of the six equations is sufficient to fully-define the initial value problem.

For all the following we integrate this coupled system of equations using the backward Euler method in *pyoptmat*, an open source framework for simulating and calibrating ODE material models developed at ANL [6, 7, 8, 9]. Numerically integrating these ODEs for times t_i gives a time series of the values $\sigma_{1,i}$, T_i, d_i, $K_{1,i}$, $K_{2,i}$, and $K_{3,i}$ for $i \in [0, n_{time}]$ where the values at $i = 0$ are the initial conditions.

We are interested in the mechanical strain in bar 1, in addition to the stress. We can obtain the mechanical strain by numerically integrating the mechanical strain rate of bar 1, defined as

$$\dot{\varepsilon}_{mech,1} = \frac{\dot{\sigma}_1}{E_1'} + \dot{\varepsilon}_{in,1} \tag{2.30}$$

through the integrated time series giving the stress (σ_1), damage (d), and isotropic hardening (K_1) values for bar 1. We implement this numerical integration with a simple right Riemann sum.

2.2.3 Synthetic data

We now have a means to simulate deformation and damage in surveillance articles. We will use this capability to generate synthetic test data, replicating actual testing of the surveillance article in either a reactor environment or a furnace. To generate this synthetic test data we use the Larson-Miller damage model for the test section, to represent the accumulation of creep damage in the test article during service.

Figure 2.5 shows the temperature history used to simulate in reactor degradation of the test material. This consists of a ramp from 300° C to 650° C over 1 hour, a hold at constant

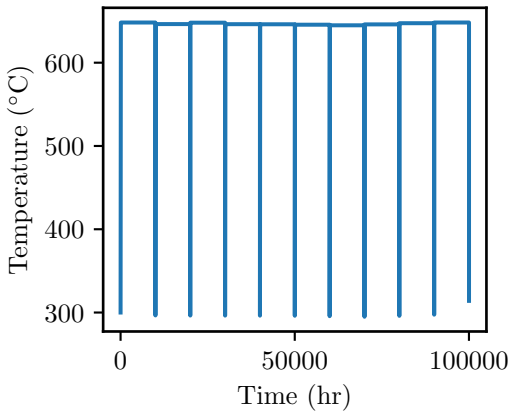

Figure 2.5: In service temperature history.

temperature for 10,000 hours, and a ramp back down to 300° C over 1 hour. This cycle might represent the transition between a hot standby and steady operating conditions in a reactor.

One advantage of simulating synthetic test data is we have complete information on the state of the test material during "service", which will be unavailable for actual surveillance programs. Figure 2.6 plots the mechanical strain versus time, the stress versus time, and stress/mechanical strain hysteresis, and, most interestingly, the accumulated damage in the test article over time.

The damage versus time plot provides a benchmark to assess methods to infer the state of damage in the specimen from information that can be collected ex-situ on post-service samples. The final damage fraction for this sample after 100,000 hours of service is 0.35. If we can infer that level of damage from (simulated) ex-situ testing we have a viable approach to accomplish the key goal of this work.

2.2.4 Simulating ex-situ testing

Again, we replace actual ex-situ testing of post-service samples with simulations. To accomplish this we start from the material state of the simulated in service samples, specifically the values of damage d and isotropic hardening K_1, K_2, and K_3 and impose an additional, shorter temperature history that might represent out-of-reactor instrumented furnace testing.

Figure 2.7 plots the ex-situ thermal history, which consists of a 1 hour ramp from 300° C to 650° C, a hold at constant temperature for 1 hour, and a ramp back down to 300° C over 1 hour. To some extent this ex-situ test cycle is arbitrary, but it should meet two criteria:

1. It should include a large enough temperature difference to induce measurable stress relaxation in the test section. A small strain range in the elastic regime may not provide enough information to infer damage. Similarly, the hot end of the cycle should be in the creep regime.

2. It should have a relatively short duration. The reactor operator will likely want to determine the component remaining life during a service outage with a time on the

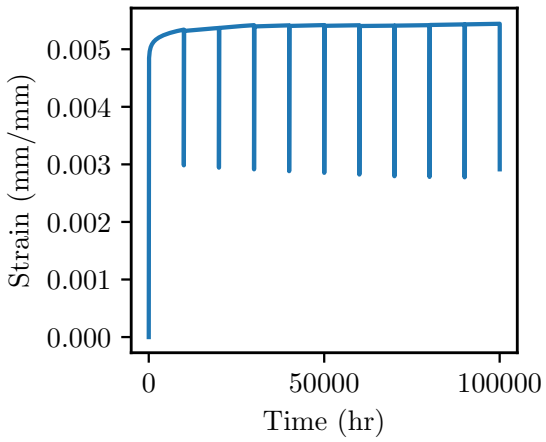

(a) Mechanical strain versus time.

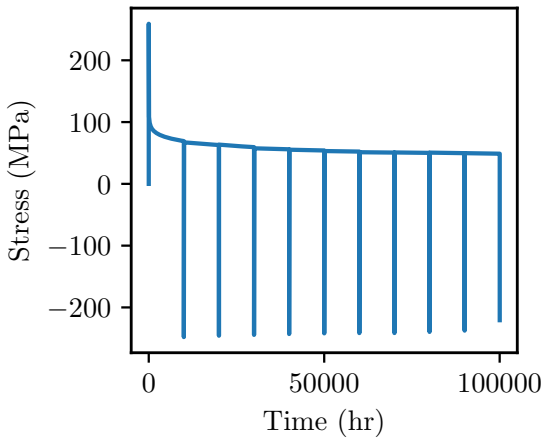

(b) Stress versus time.

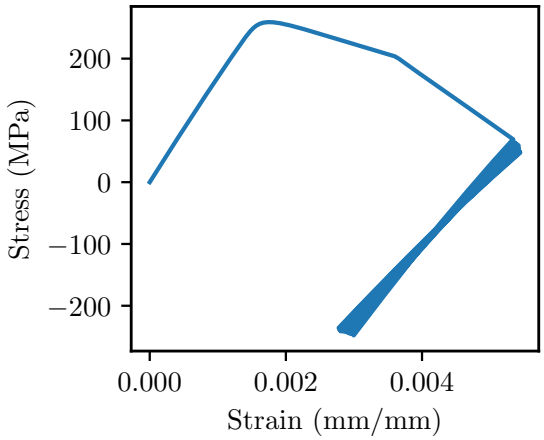

(c) Stress/strain hysteresis.

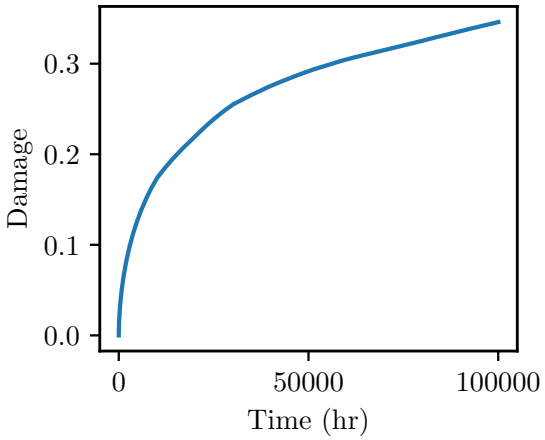

(d) Accumulated creep damage versus time.

Figure 2.6: Simulated data for the in-service test article.

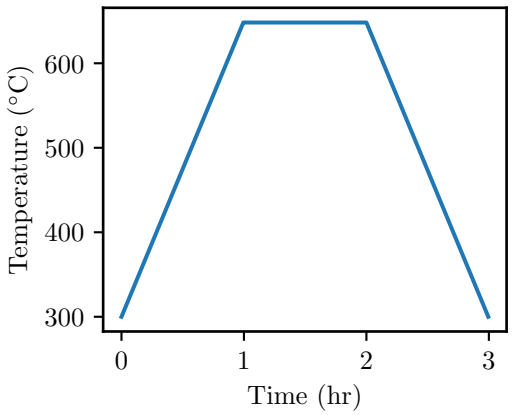

Figure 2.7: Ex-situ test temperature history.

order of a few weeks. The sample will have to rest to reduce its level of radiation before it can be tested and so the furnace/mechanical testing should be as short as possible.

Because we are simulating this ex-situ testing, Figure 2.8 reports full information (stress versus time, strain versus time, and stress-train hysteresis) for the test section of the sample. However, the only data that will be easily available in an actual test is the strain versus time (Figure 2.8a) signal. As such, in the following we assume we only have this data available to infer damage in the sample.

2.3 Inferring damage

The key question is if we can infer the current damage fraction in the sample, d, from the ex-situ strain versus time data shown in Figure 2.8a. If we can infer the current state of damage we can also use a damage model to predict the remaining life of the test section material and, by inference, the remaining life of the monitored component.

2.3.1 General procedure

We can pose the challenge of inferring damage from the strain signal as a shooting problem. We can simulate the response of the specimen under the ex situ thermal loading history and try to find the initial value of the damage parameter d in the test section and the unknown current material state, here the level of isotropic hardening K, in all three sections of the sample, and the initial (residual) stress in bar 1, σ_1. The remaining initial condition is the initial value of temperature, which is known from the imposed thermal cycle in Figure 2.7.

The goal of this optimization problem is to find the initial state of the material, including the damage fraction, so that the simulated strain history matches the experimental strain history. We formally pose the optimization problem with a root mean square loss function on the experimental strains $\varepsilon_{exp,i}$ and the simulated strains $\varepsilon_{sim,i}$ as:

$$y_{opt} = \arg\min_{y_0} \sum_{i=1}^{n_{time}} \left(\varepsilon_{exp,i} - \varepsilon_{sim,i}\right)^2 \tag{2.31}$$

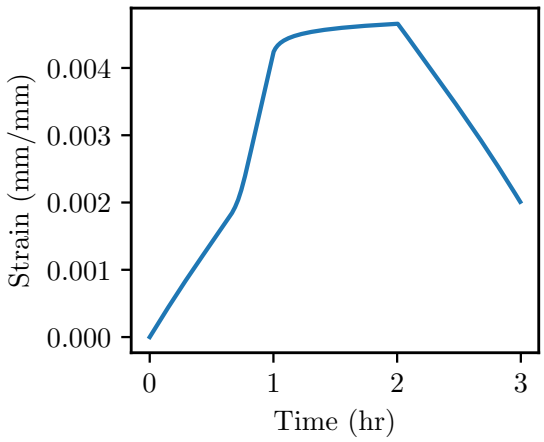

(a) Mechanical strain versus time.

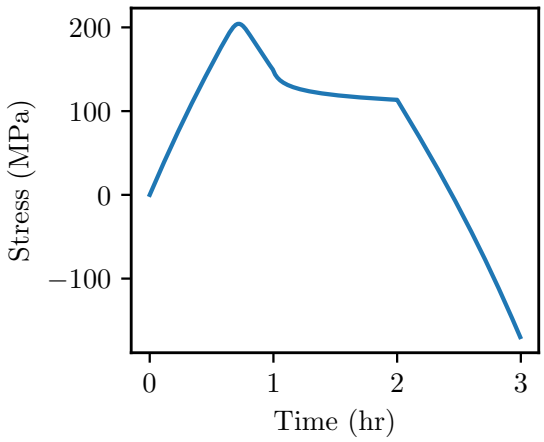

(b) Stress versus time.

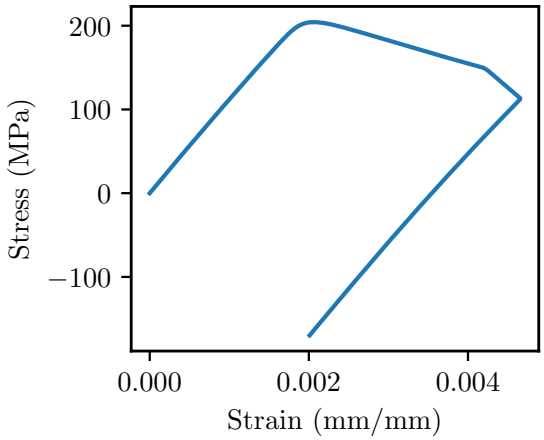

(c) Stress/strain hysteresis.

Figure 2.8: Simulated data for ex situ testing of a post-service surveillance article.

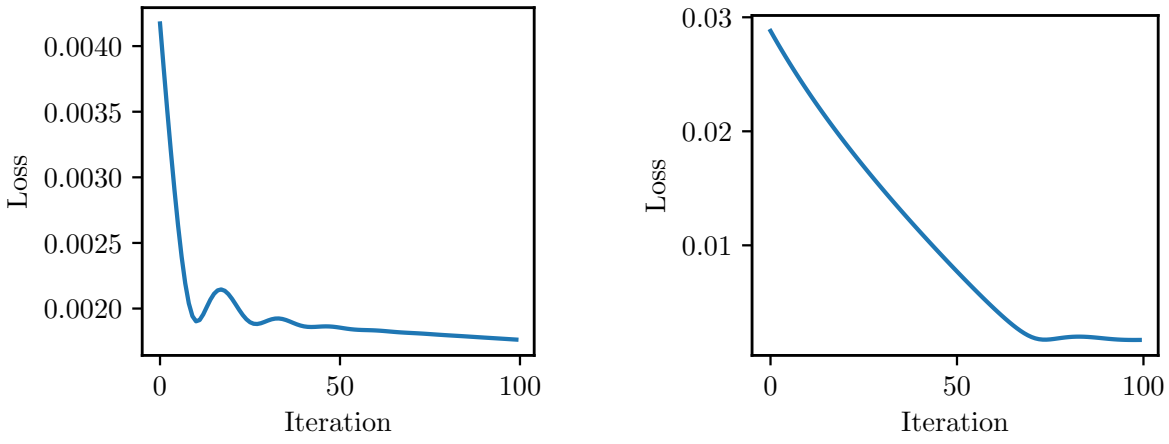

(a) Larson-Miller damage.

(b) Constant damage.

Figure 2.9: Loss histories for the optimization with the Larson-Miller (a) and constant (b) damage models.

where y_opt is the vector containing the initial conditions representing the material state $\sigma_{1,0}$, $K_{1,0}$, $K_{2,0}$, and $K_{3,0}$ and n_{time} is the number of discrete observations of the strain in the experiment (i.e. set by the data collection frequency).

We solve this optimization problem using *pyoptmat* by applying the Adam gradient-descent optimizer. Our previous work describes how *pyoptmat* can efficiently solve ODE-based optimization problems of this type, including how the software parallelizes the calculations on the GPU and applies the adjoint method to efficiently calculate the gradient of the loss function with respect to the parameters.

In simulating the response of the sample we consider two different damage models:

1. The actual Larson-Miller damage model used to simulate the response of the sample (Eq. 2.15).

2. The constant damage model (Eq. 2.11).

In the first case we assume that damage accumulates during the ex situ thermal cycling and we know, a priori, how the sample accumulates creep damage. In the second case we assume that no damage accumulates during the ex situ loading but we need to make no assumptions on how the material accumulates creep damage. The following compares the accuracy of both approaches and the subsequent discussion describes the advantages of disadvantages of each.

2.3.2 Results

We solved the shooting problem with a learning rate of 10^{-3} and 100 iterations of the Adam optimizer. Figure 2.9 plots the convergence history for both cases described in the previous section. The optimizer successfully finds a local minima for both damage models.

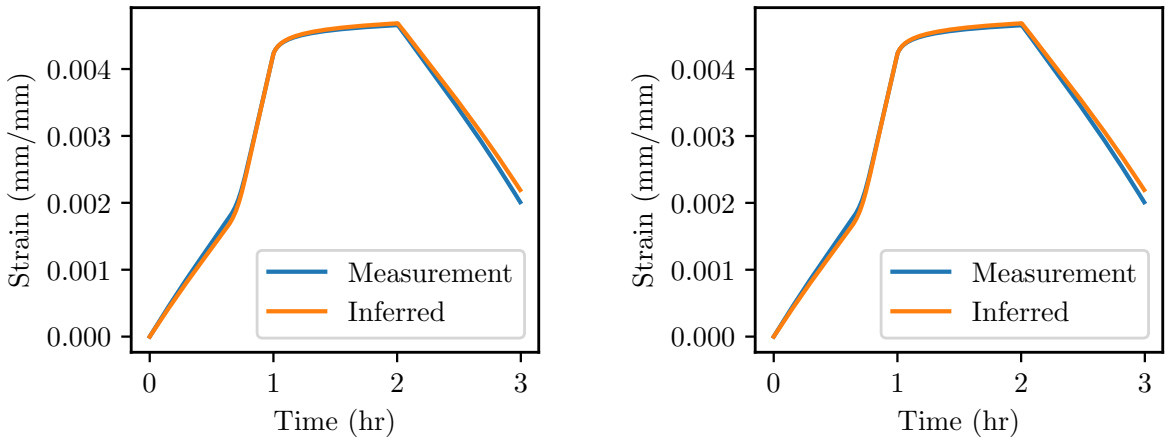

(a) Larson-Miller damage.

(b) Constant damage.

Figure 2.10: Calibrated strain histories solving the shooting problem for the initial material state for the Larson-Miller (a) and constant (b) damage models.

	$d_{inferred}$	d_{actual}	Error
Larson-Miller	0.27	0.34	21%
Constant	0.28	0.34	18%

Table 2.4: Tabulated values of the inferred damage and the error between the calibrated and inferred values.

Figure 2.10 plots the optimal simulated versus "experimental" (here synthetically generated) ex situ strain history. The strain versus time trajectory for the optimized initial state accurately matches the experimental strain signal.

Finally, Table 2.4 compares the actual, ground truth value of the damage parameter to the optimized value for the two cases. The approach accurately recovers the amount of creep damage the material accumulated in service.

2.3.3 Discussion

This numerical approach can reliably and accurately calculate the amount of damage accumulated in a test article, given only a description of the undamaged material behavior (the deformation model) and ex situ measurements of the strain in the test section. This approach could be used to calculate the amount of damage, and therefore the remaining life, for actual test articles exposed to the in situ MSR environment.

We repeated the optimization for the damage fraction several times starting from different initial values for the residual stress, the prior damage, and the isotropic hardening. The method reliably calculates nearly the same optimized prior damage, regardless of the starting conditions. However, the values of the initial residual stress and the initial isotropic hardening are less reliable and more sensitive to the initial guesses. This implies the simulations are not sensitive to these values. For isotropic hardening this is because the material

has exhausted most of its work hardening by the point of the ex situ test and behaves nearly perfectly viscoplastic.

It is less clear why the results are insensitive to the residual stress in the test section. However, we can view this favorably as it suggests the residual/mean stress does not significantly affect strain accumulation and damage during the in situ loading.

There is basically no difference in accuracy between inferring from the actual Larson-Miller damage model and the constant damage model. This may be because the ex situ load cycle was short enough to not add any additional damage to the specimen. A longer ex situ cycle might contribute additional damage, meaning the Larson-Miller model may become more accurate. However, given that one of the objectives for the ex situ loading cycle is to have a short duration, we recommend proceeding with the constant damage approach, as it requires less prior material information.

3 Modeling support for INL's experimental campaign

3.1 Effect of shutdowns on damage accumulation

The thermal cycle applied in Chapter 2 is not fully realistic: the specimen will need to come to room temperature at least to be removed from the plant component and moved to a location for the post-service testing. This large thermal cycle must occur at least twice — when the specimen is first inserted into the reactor and/or when the reactor first starts up and when the specimen is removed for testing. It may occur more often. For example, the component may come to room temperature naturally during plant outages or specimens may be removed, non-destructively tested, and reinserted into the reactor.

This large thermal transient will affect the accumulation of creep and fatigue damage in the specimen. To assess this effect we completed a numerical study with the three bar model of the test article described in Chapter 2. The geometry of the test article and the material models are the same as in that chapter. The difference is the thermal cycle. Now the overall thermal history of the sample includes two types of cycles:

1. A ramp from room temperature (20° C) to 500° C over 1 hour and a return to room temperature over the same amount of time.

2. A ramp from 500° to 550° C over 1 hour, a hold at 550° C for 1,000 hours, and a ramp back to 500° C over one hour.

Each cycle type 1 (N) contains one or more repetitions of cycle type 2 (N_p). However, we keep the product of NN_p constant so that the total time of the entire thermal load history remains approximately constant. Figure 3.1 shows an example of this temperature history for $N = 16$ and $N_p = 5$.

Figure 3.2 then plots the simulated damage and stress in the test article as a function of time for several combinations of N and N_p.

Increasing the number of room temperature excursions increases the creep damage accumulated in the sample. The large temperature change induces a large mechanical strain in the test article, leading to high stresses and increased damage accumulation. As Figure 3.2b illustrates, increasing the number of room temperature transients increases the maximum stress in the sample by effectively resetting the stress relaxation. This increased stress explains the increase in creep damage.

This study suggests that a surveillance procedure will need to account for room temperature excursions in addition to the standard operating component transients. One way to account for these transients is to include the transient from operating to room temperature in the simulated history used to infer the specimen remaining life. The overall ex situ test would then effectively consist of the transient to room temperature followed by the instrumented furnace thermal cycling. The objective function would only seek to match the strains during the furnace loading, as the strains during the transient to room temperature could not be measured.

3.2 Ratcheting

If the driver or case sections of the test articles experience high enough stresses and temperatures to undergo creep then the strains in the test section will not come to some steady,

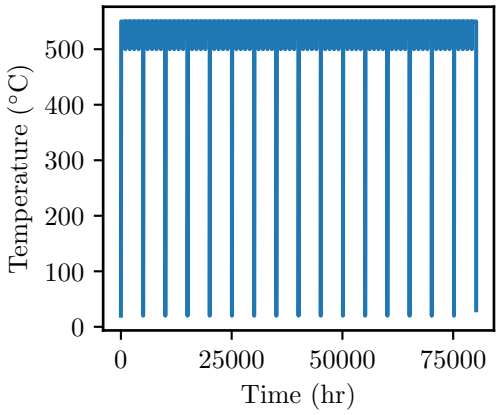

Figure 3.1: Example of a thermal cycle with $N = 16$ and $N_p = 5$.

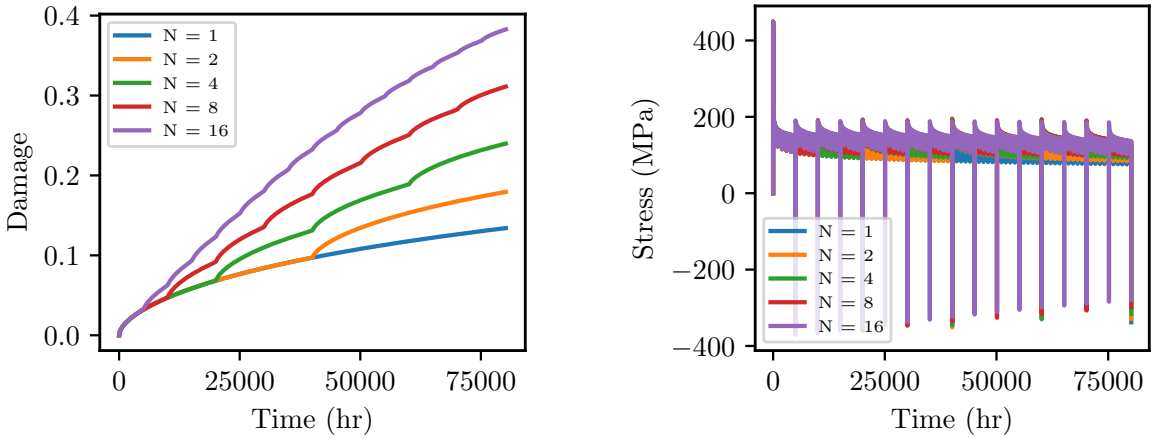

(a) Simulated damage.

(b) Simulated stress.

Figure 3.2: Simulation results for different numbers of unloading cycles.

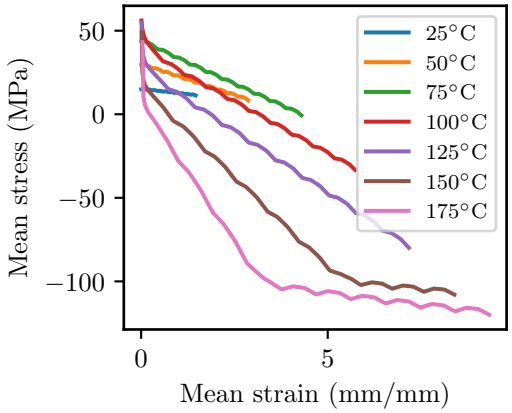

Figure 3.3: The center of the stress/strain hysteresis loops for increasing ΔT.

periodic condition. The stresses in the test section will stabilize, but that may be a slow process. The combination of these two effects will cause the stress/strain hysteresis loop experienced by the test section to wander over time. Potentially, this motion may gradually alleviate the stresses experienced by the test section, reducing the creep and fatigue damage it experiences.

Alleviating the movement of the test section stress/strain hysteresis is useful because it makes the calculation of the specimen damage more reliable as the damage per cycle does not change with time.

Figure 3.3 plots the center of the stress/strain hysteresis loop for the three bar model of the test article described in Chapter 2 as it moves with time. These simulations use a simple thermal cycle, starting at $T_0 = 500°$ C and increasing by varying ΔT values to $T_0 + \Delta T$. The temperature is held fixed for 1000 hours, then the sample cycled back to $T_0 = 500°$ C. This thermal cycle is repeated 500 times to understand the steady cyclic behavior. To avoid conflating effect we turn off the damage model for these simulations.

The larger the temperature range the farther the test section ratchets. Similarly, the larger the temperature range the faster the specimen approaches a steady stress. Interestingly, this steady stress is not centered on zero, but rather on a fairly large value of compressive stress. For small temperature ranges the change in stress from cycle to cycle is nearly negligible, but for larger temperature ranges the stress evolves fairly rapidly. However, in all cases the change in stress is small compared to the large ratcheting strain experienced by the test article.

This study suggests the specimens should be designed to minimize the ratcheting strain, which in turn minimizes the change in the mean stress. It also suggests that the test articles will inevitably experience fairly large ratcheting strains, which will have to be accommodated by the test section.

3.3 Out of plane deformation

In the idealized three bar model the large ratcheting strain is accommodated only through uniaxial deformation of the test section. In actual samples some of this axial deformation

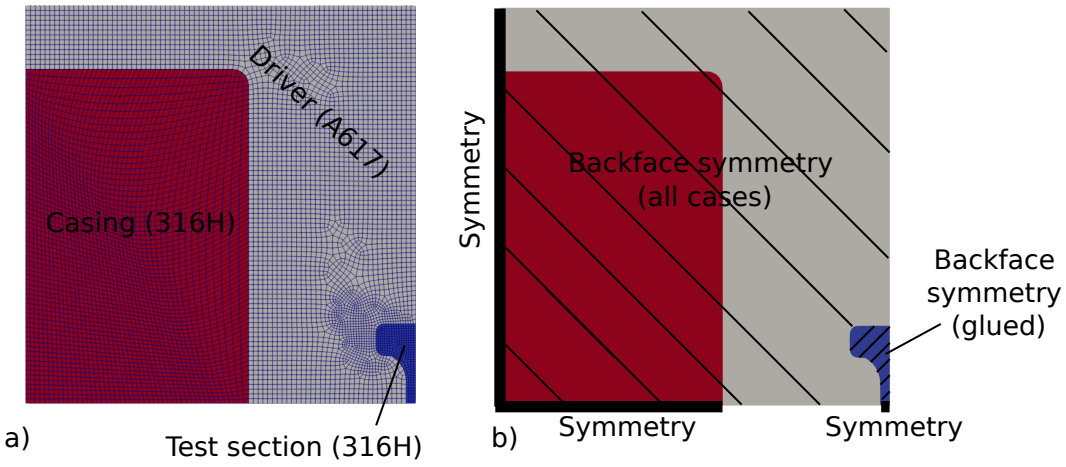

Figure 3.4: Simulation domain and boundary conditions. The specimen is 1.2 mm thick, meshed with 8 linear hex elements through the thickness. (a) Plane view of the mesh. (b) Boundary conditions, showing in particular the difference between the glued and free simulations.

can be translated to bending out of plane deformation, especially if the original sample is prone to lateral instability.

We simulated the response of the flat specimen currently under development at INL [3] to assess what effect this out of plane bending might have on the effective axial response of the test section. The flat specimens is especially vulnerable to incremental out of plane ratcheting, as its thin aspect ratio promotes lateral instability.

Figure 3.4 shows the computational model with the applied boundary conditions. We consider two cases: one where the test section can move out-of-plane, as in the real tests, and a second where the test section is "glued" to the bottom surface. This model does not include the slot separating the two driver sections, present in the real sample. Instead the symmetry boundary condition only applies to the test and casing sections, representing the disconnect caused by the physical slot.

To represent the effect of misalignment of the test section we tilt the gauge portion of the test section 3° out of alignment with the rest of the test article. This represents potential actual misalignment plus induces localizaton of progressive out of plane deformation/ratcheting to the test section.

We use a variant of the material models for 316H and Alloy 617 discussed in Chapter 2. These simulations do not include damage in the test section. Figure 3.5 shows the thermal cycle used in the analysis. This thermal cycle was selected to induce large strains in the test article. The analysis could be repeated in the future for small temperature ranges.

Figure 3.6a then plots the out of plane displacement on the outside surface of the test section gauge, at the symmetry plane, as a function of time. This displacement is zero for the "glued" model, by construction. The free model progressively develops increasing out of plane deformation as the test section gauge bends out of alignment with the driver and

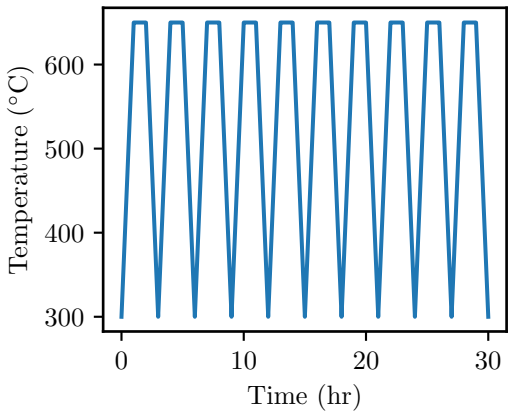

Figure 3.5: Temperature history for the out-of-plane bending study.

casing sections (see Figure 3.6b).

Finally, Figure 3.7 plots the difference between the free and glued simulations by showing the axial stress stress hysteresis loops over the gauge of the test section for both simulations. This plot shows the effect of the out-of-plane deformation on the axial stress and strain delivered to the gauge section. As this stress is ultimately what causes failure of the test article, this plot assess the practical effect of the out-of-plane bending.

The effect of the out-of-plane bending is primarily on strain accumulation and even there the effect is small. The stress/strain histories for the two cases are different, with the free case accumulating somewhat more ratcheting strain. However, over 10 cycles these differences are comparatively small. These simulations could be continued to larger cycle counts to ascertain the long-term difference in response. However, this case deliberately applied a large temperature differences so it might take many thousands of cycles for significant differences to appear for more reasonable temperature ranges.

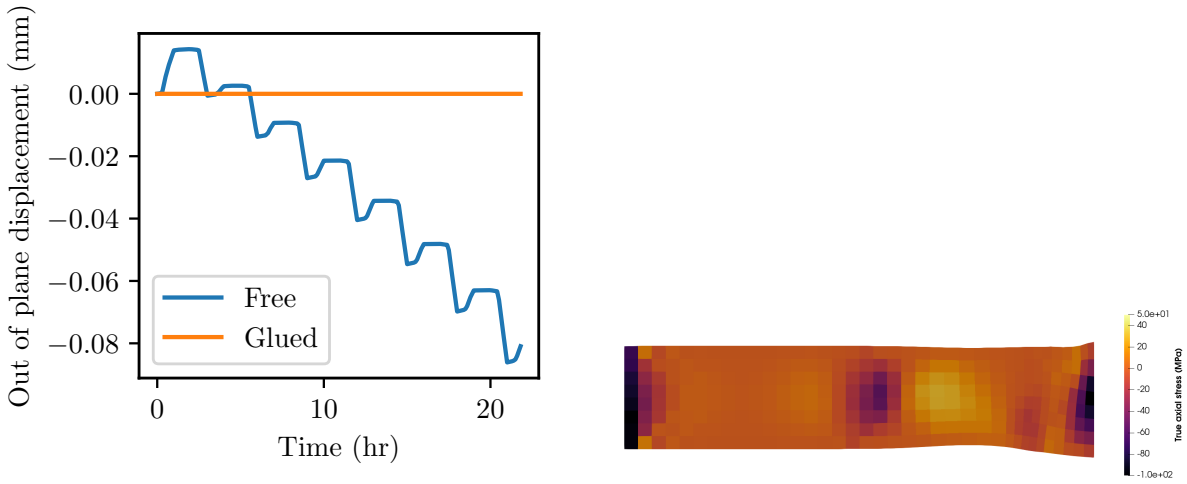

(a) Out of plane ratcheting.

(b) Side view of deformed, bent specimen..

Figure 3.6: (a) Out-of-plane ratcheting displacement for the two simulations. (b) Side view of the deformed shape for the free case. This snapshot is at the peak tensile load on the test section, showing residual bending as the thermal strain straightens the test section. The fringe colors show the axial stress.

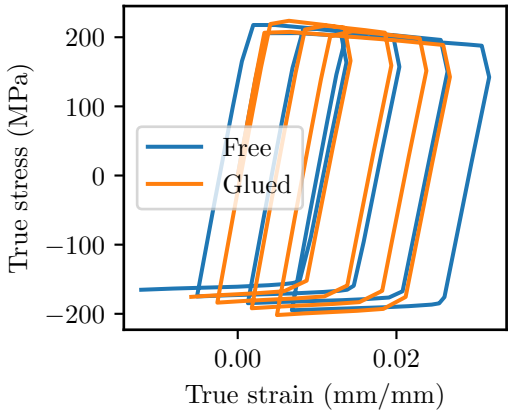

Figure 3.7: Comparison between the free and glued simulations of the INL flat specimen showing the effect of the out of plane displacement on the axial stress/strain hysteresis loops.

4 Conclusions

This report summarizes modeling and simulation activities at ANL in FY23, supporting the development of passively actuated mechanical surveillance test articles by the ART program. These test articles will be a vital component of a MSR material surveillance program aimed at monitoring the degradation in the performance of plant structure materials over time in future operating plants. The main focus of Argonne's work was to develop a novel approach for relating mechanical test data the specimens before and after exposure to the amount of damage accumulated in the test article during service under the reactor thermal and/or environmental conditions.

The focus of future work will be to develop the approach for inferring creep damage, described in Chapter 2, into a practical procedure plant operators can use to assess operating MSR structural components. This may require simplifications to the general approach, with a corresponding reduction in the accuracy of the predictions, to make it easier to implement in an operating environment. This also requires work to flesh out the basic method into a complete procedure for sizing, locating, and testing surveillance articles. This will include techniques for determining the appropriate specimen design and location for monitoring a particular component and general guidelines for how many surveillance articles might be required to monitor a particular component over a particular period of time. It will also include developing more detailed test procedures, including guidance on how frequently to remove and test specimens and if specimens can be reused by reinserting them into the operating component. Finally, it will also require defining definite acceptance procedures formulated by relating the predicted remaining life of the component to the original design life.

Acknowledgements

This work was sponsored by the U.S. Department of Energy, under Contract No. DE-AC02-06CH11357 with Argonne National Laboratory, managed and operated by UChicago Argonne LLC. Programmatic direction was provided by the Office of Nuclear Reactor Deployment of the DOE Office of Nuclear Energy.

The authors gratefully acknowledge the support provided by Sue Lesica, Federal Manager, Advanced Materials, Advanced Reactor Technologies (ART) Program, Brian Robinson, Federal Program Manager, ART Molten Salt Reactors (MSR) Campaign, and Patricia Paviet of the Pacific Northwest National Laboratory, National Technical Director, ART MSR Campaign as well as the technical guidance provided by Sam Sham of Idaho National Laboratory.

Bibliography

[1] M. C. Messner, Y. Momozaki, and E. Boron, "Report on thermal cycling testing and bimaterial weld development for a passively actuated materials surveillance test article," Tech. Rep. ANL-ART-245, Argonne National Laboratory, 2022.

[2] M. C. Messner, Y. Momozaki, E. Boron, G. Ye, and T.-L. Sham, "Fabrication and testing of two passively actuated creep-fatigue surveillance test articles," Tech. Rep. ANL-ART-228, Argonne National Laboratory, 2021.

[3] M. D. McMurtrey, H. P. Mahajan, M. N. Cinbiz, K. A. Novich, T. L. Phero, T. W. Walters, and T.-L. Sham, "Phase ii development of the surveillance test articles to improve the design, fabrication, and testing," Tech. Rep. INL/RPT-22-69281, Idaho National Laboratory, 2022.

[4] M. Messner, V.-T. Phan, and T.-L. Sham, "Evaluating and modeling rate sensitivity in advanced reactor structural materials: 316H, Gr. 91, and A617," International Journal of Pressure Vessels and Piping, vol. 178, p. 103997, 2019.

[5] H. Mecking, B. Nicklas, N. Zarubova, and U. Kocks, "A "universal" temperature scale for plastic flow," Acta Metallurgica, vol. 34, no. 3, pp. 527–535, 1986.

[6] T. Chen and M. C. Messner, "Initial development of viscoplastic constitutive model of Alloy 800H in support of the use of inelastic analysis methods for ASME Section III, Division 5, Class A applications," Tech. Rep. ANL-ART-250, Argonne National Laboratory, 2022.

[7] T. Chen and M. C. Messner, "Uncertainty quantification of visco-plastic constitutive model parameters using a hierarchical bayesian framework," Submitted for publication, 2023.

[8] T. Chen and M. C. Messner, "A universal inelastic constitutive model," in ASME Pressure Vessels and Piping Conference, pp. PVP2023–105946, 2023.

[9] T. Chen and M. C. Messner, "Training material models using gradient descent algorithms," International Journal of Plasticity, vol. 165, p. 103605, 2023.

Applied Materials Division
Argonne National Laboratory
9700 South Cass Avenue, Bldg. 208
Argonne, IL 60439

www.anl.gov